AFM and CAFM studies of ELO GaN films

V. Kasliwal[a], J.C. Moore[a], X. Ni[b], H. Morkoç[b], A.A. Baski[a*]

[a]Department of Physics and [b]Department of Electrical and Computer Engineering,
Virginia Commonwealth University, Richmond, VA 23284

ABSTRACT

The techniques of atomic force microscopy (AFM) and conductive AFM (CAFM) have been used to study the morphology and conduction properties of a-plane GaN films grown via epitaxial lateral overgrowth (ELO). Four GaN samples were prepared using metal organic chemical vapor deposition (MOCVD) with slightly different growth conditions. In AFM images, the coalesced ELO films show undulations, where the window regions appear as depressions with a higher defect density than surrounding areas. At reverse bias above 20 V, lower quality samples show localized leakage defect sites inside the window regions, whereas higher quality samples show no localized leakage. This behavior is consistent with previous observations on non-ELO samples where significantly enhanced localized leakage occurs at voltages above 15 V. Surface oxidation was also observed, where continuous scanning at reverse bias results in decreased conduction. This CAFM study confirms that ELO-grown GaN samples show enhanced reverse-bias leakage inside window regions where a higher defect density is present.

Keywords: GaN, AFM, CAFM, a-plane, epitaxial lateral overgrowth, leakage

1. INTRODUCTION

Device fabrication has been hampered in GaN films by the presence of localized regions exhibiting reverse-bias leakage. As shown in CAFM studies, films grown via molecular beam epitaxy (MBE) can have "hillock" topographical features that demonstrate leakage behavior which is usually associated with screw-like dislocations.[1,2,3] The mechanism responsible for such leakage is still debated and has been attributed to excess Ga incorporation or oxygen-related impurities in the vicinity of screw dislocation cores.[4,5] Edge and screw dislocations have also been imaged by techniques such as scanning Kelvin probe microscopy (SKPM) and scanning capacitance microscopy (SCM).[6,7,8] Edge dislocations show an intrinsic negative charge with no associated reverse-bias leakage,[9] whereas screw-like dislocations demonstrate leakage with no inherent charge.[3] Therefore, no strong correlation exists between charged dislocations and localized reverse bias leakage. Local I-V behavior in the vicinity of defect regions has shown discernible differences in both forward and reverse bias for films grown on hydride vapor phase epitaxy (HVPE) and MOCVD templates.[1,10,11] Reverse bias conduction has been attributed to mechanisms such as Frenkel-Poole conduction, field-emission and trap-assisted tunneling, or 1D hopping associated with threading dislocations.

The majority of electronic studies have concentrated on dislocations for the polar, c-plane of GaN. However, strain-induced piezoelectric effects and spontaneous polarization both produce electric fields that can introduce additional device constraints for this orientation.[12,13] More recently, the non-polar, a-plane of GaN has gained attention.[14,15,16] Growth techniques such as epitaxial lateral overgrowth (ELO) and sidewall ELO of a-plane GaN have shown a decrease in the dislocation density for films grown via MOCVD[17,18,19] and HVPE.[20] Dislocations bend out from the window regions during ELO to achieve minimum energy, resulting in a reduced number of threading dislocations terminating on the surface.[21] Counter-propagating dislocations from opposing wings may also annihilate. The films therefore have a lower overall density of dislocations, with the majority of the dislocations occurring in the window vs. wing regions. Recent CAFM and near-field scanning optical microscopy (NSOM) studies indicate that localized reverse-bias leakage in such films is usually confined to the window regions.[22] Time-resolved photoluminescence studies also show that GaN films grown via ELO demonstrate a significant increase in material quality.[23,24] In this study, we have used CAFM to examine the structural and electronic properties of a-plane GaN films grown via MOCVD using the ELO technique. Specifically, we compare films grown via single- and two-step processes, and discuss how sample quality, III/V ratio, and doping affect the reverse-bias leakage behavior.

---

[*] aabaski@vcu.edu; phone 1 804 828-8295; fax 1 804 828-7073

2. EXPERIMENTAL

In this study, the templates for ELO growth consist of a-plane (11$\underline{2}$0) GaN films (1.5 μm) grown by MOCVD at 1050 °C on r-plane (1$\underline{1}$02) sapphire substrates. To form the ELO pattern, a 100 nm-thick SiO_2 layer was deposited via plasma-enhanced chemical vapor deposition, and then patterned with 4 μm wide windows oriented parallel to the m-direction [1$\underline{1}$00] (14 or 24 μm pitch) using conventional photolithography and buffer oxide etching. The ELO samples for this study were subsequently grown under various parameters (see Table 1) and have the following designations: sample A (cvd947), sample B (cvd1089), sample C (cvd1056), and sample D (cvd1242).

A single-step growth process was used for sample A; however, difficulties in coalescence arise due to differences in wing tilt between the Ga- and N-polar wings.[25] Recent TEM studies indicate that a two-step process results in more uniformly coalesced ELO a-plane films,[19] which is utilized for the growth of samples B, C, and D. The trimethylgallium (TMG) flow rate is constant for all four growths, but the NH_3 flow rate is decreased in the second stage for sample C, resulting in a higher III/V ratio. Growth parameters for sample D are identical to those for sample B, but the film is Si-doped to increase conductivity.

Table 1: Growth conditions for four samples discussed in this study.

	Sample A	Sample B		Sample C		Sample D	
	Stage I	Stage I	Stage II	Stage I	Stage II	Stage I	Stage II
Si Doping Level (cm^{-3})	0	0	0	0	0	2×10^{16}	2×10^{16}
TMG (μmol/min)	157	157	157	157	157	157	157
NH$_3$ (sccm)	510	3000	3000	3000	560	3000	3000
Growth Duration (h)	5	2	3	2	3	2	3
Temperature (ºC)	1050	1000	1050	1000	1050	1000	1050

AFM and CAFM data were acquired using a Veeco Dimension 3100 AFM with Si cantilevers for high-resolution tapping-mode topography, and Ti/Pt-coated cantilevers for electrical characterization. For CAFM data acquisition, ohmic contacts were formed on all samples using Ti/Al/Ti/Au metallization, and a microscopic Schottky contact existed between the metallized CAFM tip and sample. Bias voltages were applied to the sample with the tip at ground, and current measurements were obtained using a current amplifier module with a range of 1 pA to 1 μA. For high voltage studies (>12 V), an external bias voltage was applied to the sample using a selectable battery source.

3. RESULTS

The three samples grown via a two-step process (B, C, and D) show undulating surface topographies, where the windows are distinctly visible as depressions in the topography and exhibit a higher density of surface pits in comparison to wing regions. For sample A, however, the window and wing regions are indistinguishable in AFM images, and the overall surface roughness is increased. The relative quality of these samples also vary, where samples A and B are qualitatively better than C and D, as determined by CAFM, NSOM, and x-ray diffraction (XRD) studies. Below, we discuss differences in defect densities between the wing and window regions, and examine the reverse-bias leakage behavior as a function of sample quality.

3.1 Window vs. wing topography

The difference in topography between the window versus wing regions is evident in Fig. 1, where a high-resolution, tapping-mode AFM image of sample C is shown in (a). To enhance features in the window region, Fig. 1(b) is the corresponding high-pass filtered image with a Sobel edge enhancement that produces dark pixels at edge features. The window region (highlighted by black lines) appears as a dark band in the processed image, indicating a high density of edges at surface pits (~ 6 to 8 nm deep). The Ga- and N-wings seen on either side of the window have significantly fewer edges and corresponding defects. This difference in wing vs. window morphology has been observed in previous studies, where an increase in defect density has been seen both in the window regions and at the wing meeting fronts.[17,22]
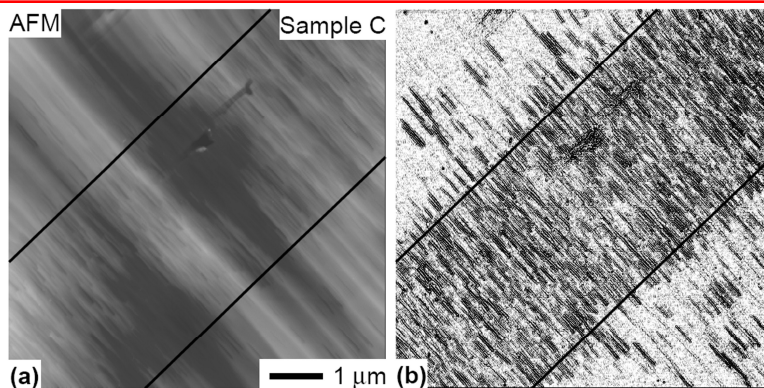
Fig. 1 (a) Tapping-mode AFM topography image ($7{\times}7\ \mu m^2$, grayscale range = 50 nm) of sample C and its (b) high-pass filtered and Sobel edge-enhanced image. The window region is highlighted by black lines.

3.2 CAFM studies of higher quality ELO GaN samples

CAFM current maps show a distinct difference between samples with respect to quality. Figure 2 includes contact-mode AFM images with their corresponding CAFM current maps for the higher quality samples A and B. Although Sobel processed images (not shown) indicate a higher density of edges in window regions (highlighted by black lines), there is no prevalence of localized reverse bias leakage in these regions at defects. As seen in Fig. 2(b), sample A has enhanced uniform reverse bias conduction in the wing regions, whereas sample B [Fig. 2(d)] shows only slightly enhanced conduction in the window regions. The difference in conduction current between the wing and window regions is extremely small for both sample A (1.4 pA) and sample B (60 fA).
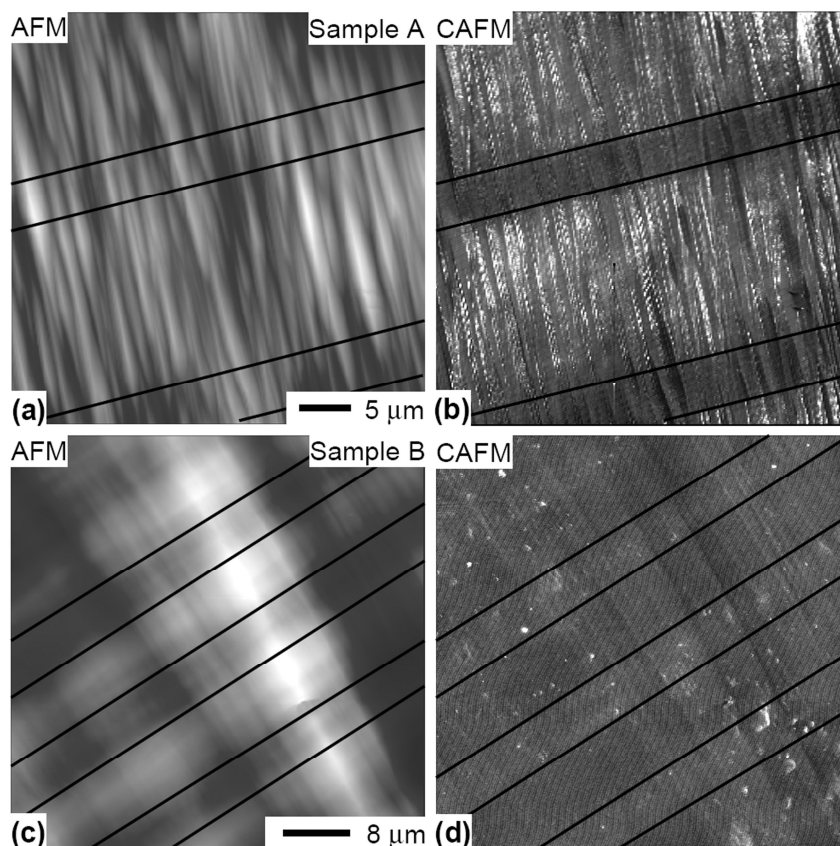

Fig 2. (a) AFM ($40{\times}40\ \mu m^2$, grayscale range = 500 nm) and (b) corresponding CAFM (48 V, grayscale = 8 pA) images of sample A. (c) AFM ($50{\times}50\ \mu m^2$, grayscale = 300 nm) and (d) CAFM (56 V, grayscale = 2 pA) images of sample B.

3.3 CAFM studies of lower quality ELO GaN samples

Figure 3 includes CAFM images of the lower quality samples C and D. Sample C has slightly enhanced uniform reverse bias conduction in the window regions [Fig. 3(b)], whereas such conduction occurs in the wing regions for sample D [Fig. 3(d)]. Hence, the uniform conduction behaviors of the films in this study do not appear to correlate with sample quality. However, these lower quality samples do exhibit localized, reverse-bias leakage sites in the window regions with relatively large currents of up to 5 nA (sample C) and 100 pA (sample D). The densities of such leakage sites within the window regions are similar for sample C (1.8×10^7 cm^{-2}) and sample D (1.2×10^7 cm^{-2}), and are comparable to that seen for MBE on MOCVD GaN films.[26] The location of leakage sites in the window regions indicates lower film quality for samples C and D, where surface pits could be decorating threading dislocations that exhibit high leakage current.
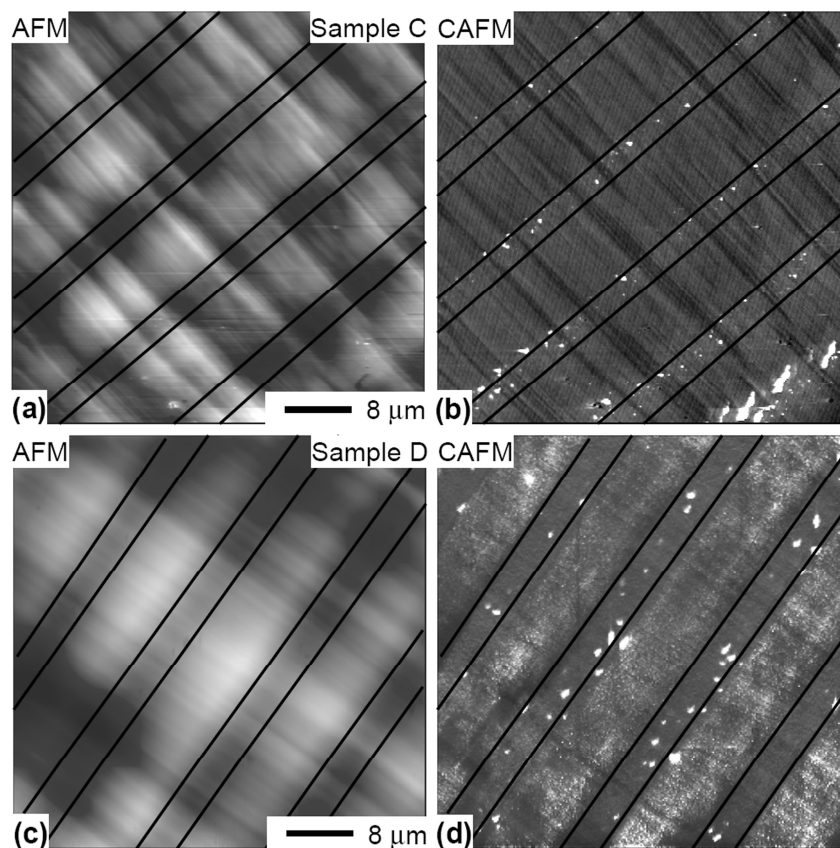

Fig 3. (a) AFM (50×50 μm^2, grayscale range = 100 nm) and (b) corresponding CAFM (30 V, grayscale = 5 pA) images of sample C. (c) AFM (50×50 μm^2, grayscale = 200 nm) and (b) CAFM (45 V, grayscale = 20 pA) images of sample D .

The observed leakage behavior of the lower quality samples C and D may be related to their growth conditions. Sample C was grown with a higher III/V ratio and therefore incorporates more Ga metal as compared to the higher quality samples. As mentioned earlier, excess Ga incorporation in the vicinity of screw dislocations can possibly lead to leakage defects.[4] Sample D had the same III/V conditions as the higher quality samples, yet exhibits localized reverse bias leakage. This behavior may result from the incorporation of Si dopants (~2×10^{16} cm^{-3}) into the film.

All four samples in this study exhibited relatively high resistance with no discernable forward-bias turn-on voltage up to ~60 V. However, the lower quality films did show forward bias conduction at defect regions. Figure 4 includes a contact-mode topography of sample C with corresponding CAFM current images under reverse and forward bias. The locations of the conduction sites under forward bias in Fig. 4(c) coincide with those for leakage sites in Fig. 4(b), suggesting that localized forward- and reverse-bias conduction can be attributed to the same current pathway.
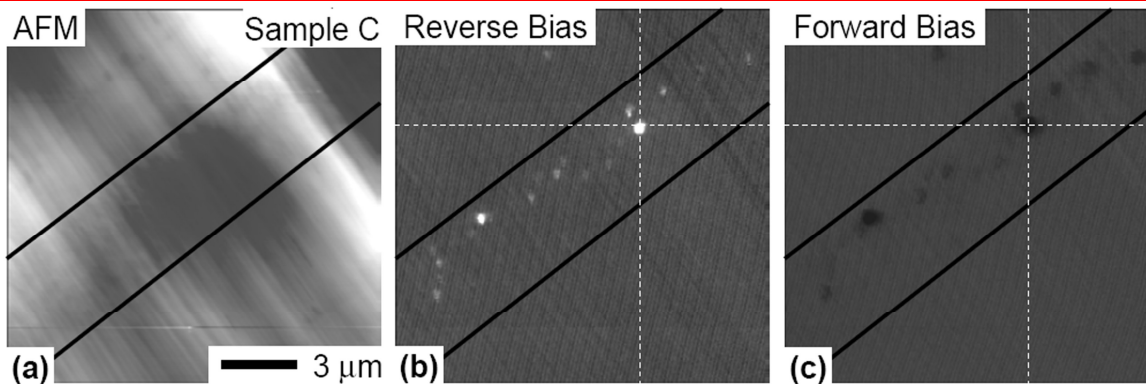
Fig 4. (a) AFM image (15×15 μm^2, grayscale range = 80 nm) of sample C with corresponding CAFM current maps for (b) reverse bias (30 V, grayscale = 5 pA) and (c) forward bias (-30 V, grayscale = 10 pA).

3.4 Tip-Induced Oxide Growth

It should be noted that the CAFM data shown for all samples were acquired during the initial scan of the sample area. Sequential scans of any regions exhibiting current conduction show substantially decreased conductivity after the first scan, which has been documented in previous work.[26] Figure 5 includes an AFM image of sample A with its corresponding reverse-bias CAFM current map. A region with lower current is clearly visible as a rotated square in the upper right area of Fig. 5(b). The square region was formed by scanning this smaller area multiple times prior to acquisition of the larger CAFM image in Fig. 5(b). A decrease in current of 5.4 pA is observed in the square region. This behavior has been observed previously for localized leakage sites, and has been attributed to local oxidation of the surface under ambient conditions.
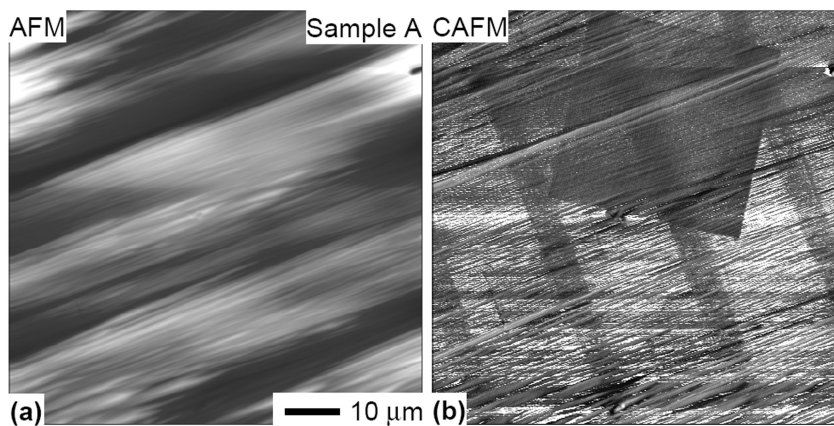

Fig. 5: (a) AFM image (75×75 μm^2, grayscale = 600 nm) and (b) corresponding CAFM current map (48 V, grayscale = 10 pA) for sample A. Prior to data acquisition, a smaller region in the upper right corner [see dark rotated box in (b)] was scanned several times under reverse bias and consequently became less conducting.

4. SUMMARY

In summary, we have examined the structural and electronic properties of several *a*-plane MOCVD-grown ELO GaN films. Films grown via a two-step process showed undulating surface topographies, with windows distinctly visible as depressions with a higher density of defect structures. All samples showed some uniform conduction in either the wing or window regions, but only lower quality films exhibited localized reverse-bias leakage in the window regions. These leakage defects could have values up to 100 pA, and are therefore detrimental to device performance in the window regions. Continuous scanning in any regions with current conduction resulted in decreased conduction, presumably due to the growth of a surface oxide under ambient conditions.

REFERENCES

1. J.W.P. Hsu, M.J. Manfra, S.N.G. Chu, C.H. Chen, L.N. Pfeiffer, and R.J. Molnar, "Effect of growth stoichiometry on the electrical activity of screw dislocations in GaN films grown by molecular-beam epitaxy," *Appl. Phys. Lett.* **78**, 3980 (2001).

2. J. Spradlin, S. Dogan, J. Xie, R. Molnar, A.A. Baski, and H. Morkoç, "Investigation of forward and reverse current conduction in GaN films by conductive atomic force microscopy," *Appl. Phys. Lett.* **84**, 4150 (2004).

3. B.S. Simpkins, E.T. Yu, P. Waltereit, and J.S. Speck, "Distinguishing negatively-charged and highly conductive dislocations in gallium nitride using scanning Kelvin probe and conductive atomic force microscopy," *Mat. Res. Soc. Symp. Proc.* **743**, L2.4 (2003).

4. J.W.P. Hsu, M.J. Manfra, R.J. Molnar, B. Heying, and J.S. Speck, "Direct imaging of reverse-bias leakage through pure screw dislocations in GaN films grown by molecular beam epitaxy on GaN templates," *Appl. Phys. Lett.* **81**, 79 (2002).

5. J.E. Northrup, "Screw dislocations in GaN: The Ga-filled core model," *Appl. Phys. Lett.* **78**, 2288 (2001).

6. G. Koley and M.G. Spencer, "Scanning Kelvin probe microscopy characterization of dislocations in III-nitrides grown by metalorganic chemical vapor deposition," *Appl. Phys. Lett.* **78**, 2873 (2001).

7. B.S. Simpkins, E.T. Yu, P. Waltereit, and J.S. Speck, "Correlated scanning Kelvin probe and conductive atomic force microscopy studies of dislocations in gallium nitride," *J. Appl. Phys.* **94**, 1448 (2003).

8. P.J. Hansen, Y.E. Strausser, A.N. Erickson, E.J. Tarsa, P. Kozodoy, E.G. Brazel, J.P. Ibbetson, U. Mishra, V. Narayanamurti, S.P. DenBaars, and J.S. Speck, "Scanning capacitance microscopy imaging of threading dislocations in GaN films grown on (0001) sapphire by metalorganic chemical vapor deposition," *Appl. Phys. Lett.* **72**, 2247 (1998).

9. J. Elsner, R. Jones, M.I, Heggie, P.K. Stitch, M. Haugk, Th. Frauenheim, S. Öberg, and P.R. Briddon, "Deep acceptors trapped at threading-edge dislocations in GaN," *Phys. Rev. B.* **58**, 12571 (1998).

10. J.C. Moore, K.A. Cooper, J. Xie, H. Morkoç, and A.A. Baski, "Conductive atomic force microscopy study of MBE GaN films," *Proc. of SPIE* **6121**, 61210J-1,6 (2006).

11. E.J. Miller, E.T. Yu, P. Waltereit, and J. S. Speck, "Analysis of reverse-bias leakage current mechanisms in GaN grown by molecular-beam epitaxy," *Appl. Phys. Lett.* **84**, 535 (2004).

12. R. Langer, J. Simon, V. Ortiz, N.T. Pelekanos, A. Barski, R. Andre, and M. Godlewski, "Giant electric fields in unstrained GaN single quantum wells," *Appl. Phys. Lett.* **74**, 3827 (1999).

13. T. Deguchi, K. Sekiguchi, A. Nakamura, T. Sota, R. Matsuo, S. Chichibu, and S. Nakamura, "Quantum-confined Stark effect in an AlGaN/GaN/AlGaN single quantum well structure," *Jpn. J. Appl. Phys. Part 2-Lett.* **38** (8B), L914 (1999).

14. H.M. Ng, "Molecular-beam epitaxy of GaN/Al$_x$Ga$_{(1-x)}$N multiple quantum wells on *r*-plane (10$\underline{1}$2) sapphire substrates," *Appl. Phys. Lett.* **80**, 4369 (2002).

15. A. Chitnis, C. Chen, V. Adivarahan, M. Shatalov, E. Kuokstis, V. Mandavilli, J. Yang, and M.A. Khan, "Visible light-emitting diodes using *a*-plane GaN–InGaN multiple quantum wells over *r*-plane sapphire," *Appl. Phys. Lett.* **84**, 3663 (2004).

16. A. Chakraborty, K.C. Kim, F. Wu, J.S. Speck, S.P. DenBaars, and U.K. Mishra, "Defect reduction in nonpolar *a*-plane GaN films using in situ SiN$_x$ nanomask," *Appl. Phys. Lett.* **89**, 041903 (2006).

17. C.Q. Chen, J.W. Yang, H.M. Wang, J.P. Zhang, V. Adivarahan, M. Gaevski, E. Kuokstis, Z. Gong, M. Su, and M.A. Khan, "Lateral epitaxial overgrowth of fully coalesced *a*-plane GaN on *r*-plane sapphire," *Jpn. J. Appl. Phys. Part 2-Lett.* **42** (6B), L640 (2003).

18. B.M. Imer, F. Wu, S.P. DenBaars, and J.S. Speck, "Improved quality (11$\underline{2}$0) *a*-plane GaN with sidewall lateral epitaxial overgrowth," *Appl. Phys. Lett.* **88**, 061908 (2006).

19. X. Ni, U. Ozgur, N. Biyikli, J. Xie, A.A. Baski, H. Morkoc, and Z. Liliental-Weber, "Defect reduction in (11$\underline{2}$0) *a*-plane GaN by two-stage epitaxial lateral overgrowth," *Appl. Phys. Lett.* **89**, 262105.

20. B.A. Haskell, F. Wu, M.D. Craven, S. Matsuda, P.T. Fini, T. Fujii, K. Fujito, S.P. DenBaars, J.S. Speck, and Shuji Nakamura, "Defect reduction in (11$\underline{2}$0) *a*-plane gallium nitride via lateral epitaxial overgrowth by hydride vapor-phase epitaxy," *Appl. Phys. Lett.* **83**, 644 (2003).

21. Z. Liliental-Weber and D. Cherns, "Microstructure of laterally overgrown GaN layers," *J. Appl. Phys.* **89**, 7833 (2001).

22. J.C. Moore, V. Kasliwal, X. Ni, U. Ozgur, H. Morkoc, and A.A. Baski, "Local electronic and optical behavior of *a*-plane GaN grown via epitaxial lateral overgrowth," *Appl. Phys. Lett.* (accepted).

23. S. Jursenas, E. Kuakstis, S. Miasojedovas, G. Kurilcik, A. Zukauskas, C.Q. Chen, J.W. Wang, V. Adivarahan, and M.A. Khan, "Increase of free carrier lifetime in nonpolar *a*-plane GaN grown by epitaxial lateral overgrowth," *Appl. Phys. Lett.* **85**, 771 (2004).

24. U. Ozgur, X. Ni, Y. Fu, H. Morkoc, and H.O. Everitt, "Near-field scanning optical microscopy and time-resolved optical characterization of epitaxial lateral overgrown *c*-plane and *a*-plane GaN," *Appl. Phys. Lett.* (accepted).

25. P. Fini, H. Marchand, J.P. Ibbetson, S.P. DenBaars, U.K. Mishra, J.S. Speck, S. Nakamura, "Defect reduction in (1$\underline{1}$00) *m*-plane gallium nitride via lateral epitaxial overgrowth by hydride vapor phase epitaxy," *Appl. Phys. Lett.*, **86**, 111917 (2005).

26. J.C. Moore, J.E. Ortiz, J. Xie, H. Morkoç, A.A. Baski, "Study of leakage defects on GaN films by conductive atomic force microscopy," *J. Phys: Conf. Ser.* (accepted).

SPIE USE: _____ DB Check, _____ Prod Check, Notes: